Behavioural Brain Research 423 (2022) 113790

Contents lists available at ScienceDirect

Behavioural Brain Research

journal homepage: www.elsevier.com/locate/bbr

Behaviour-driven *Arc* expression is greater in dorsal than ventral CA1 regardless of task or sex differences

J. Quinn Lee [a,b,*], Rebecca McHugh [a], Erik Morgan [a], Robert J. Sutherland [a], Robert J. McDonald [a]

[a] Department of Neuroscience, Science Commons, University of Lethbridge, 4401 University Drive, Lethbridge, AB T1K 6T5, Canada
[b] Department of Psychiatry, Douglas Hospital Research Centre, McGill University, 6875 Boulevard LaSalle, Verdun, QC H4H 1R3, Canada

ARTICLE INFO

Keywords:
Arc
Hippocampus
Longitudinal axis
Immediate early genes
CA1
Memory

ABSTRACT

Evidence from genetic, behavioural, anatomical, and physiological study suggests that the hippocampus functionally differs across its longitudinal (dorsoventral or septotemporal) axis. Although, how to best characterize functional and representational differences in the hippocampus across its long axis remains unclear. While some suggest that the hippocampus can be divided into dorsal and ventral subregions that support distinct cognitive functions, others posit that these regions vary in their granularity of representation, wherein spatial-temporal resolution decreases in the ventral (temporal) direction. Importantly, the cognitive and granular hypotheses also make distinct predictions on cellular recruitment dynamics under conditions when animals perform tasks with qualitatively different cognitive-behavioural demands. One interpretation of the cognitive function account implies that dorsal and ventral cellular recruitment differs depending on relevant behavioural demands, while the granularity account suggests similar recruitment dynamics regardless of the nature of the task performed. Here, we quantified cellular recruitment with the immediate early gene (IEG) *Arc* across the entire longitudinal CA1 axis in female and male rats performing spatial- and fear-guided memory tasks. Our results show that recruitment is greater in dorsal than ventral CA1 regardless of task or sex, and thus support a granular view of hippocampal function across the long axis. We further discuss how future experiments might determine the relative contributions of cognitive function and granularity of representation to neuronal activity dynamics in hippocampal circuits.

1. Introduction

The hippocampus functionally differs across its longitudinal axis; exactly how to characterize this difference remains unclear. On one view, the dorsal and ventral aspect of the hippocampus support distinct behavioural processes [1–3]. Specifically, the dorsal region is said to be necessary for spatial navigation and memory, and the ventral region is important for emotional processing [2,4]. An alternative view, largely informed by the observation that place field size increases from dorsal to ventral regions, posits instead that the hippocampal longitudinal axis varies in its granularity of representation, wherein spatial-temporal resolution of representation decreases along the axis, ventrally [5–7]. However, it remains unclear to what extent each view explains variation in cellular activity dynamics across hippocampal subregions.

Some approaches to address differences in dorsal-ventral hippocampal function are to examine neuronal activity dynamics using electrophysiological, imaging, or genetic assays, such as immediate early gene (IEG) expression in tasks with different cognitive-behavioral demands. Importantly, each approach allows researchers to address hypotheses regarding neuronal activity at varying levels of explanation. While electrophysiological and calcium imaging methods afford observation of changes in neuronal firing rate and populations in smaller volumes of tissue, measurement of IEG expression allows characterization of cellular recruitment (numbers of active neurons) across entire axes of large brain structures. According to the behavioral function view, neuronal activity will vary according to changes in task demands. For example, larger neural ensembles or increased firing rates would be observed in dorsal regions during spatial navigation, and in ventral regions in tasks that require emotional processing. One interpretation of this view is that emotional tasks will drive activation of a higher numbers of cells in ventral hippocampal regions, whereas spatial tasks will drive greater recruitment dorsally. By contrast, the granularity

* Corresponding author at: Department of Neuroscience, Science Commons, University of Lethbridge, 4401 University Drive, Lethbridge, AB T1K 6T5, Canada.
E-mail address: jquinn.lee@mail.mcgill.ca (J.Q. Lee).

https://doi.org/10.1016/j.bbr.2022.113790
Received 2 September 2021; Received in revised form 31 January 2022; Accepted 6 February 2022
Available online 8 February 2022

perspective suggests a descending gradient of cellular recruitment and similar firing rates in dorsal and ventral units along the hippocampal longitudinal axis [5,8], regardless of the specific task being performed due to the lower number of cells needed to form a coarse representation of task state-space.

Work on cellular activation during open field navigation and dry-land memory tasks has demonstrated recruitment probability is greater in dorsal than ventral hippocampal subfields CA1–3 and the dentate gyrus [9,10]. Recently, we found the same effect on activation in CA1 with the IEG *Arc* during memory-guided navigation in the Morris Water Task (MWT) [11]. One group also found a similar gradient of expression in CA1 at the protein-level with cFos [12]. Several groups have reported that contextual fear conditioning augments *Arc* expression in dorsal and ventral hippocampal subfields and is necessary for contextual fear memory [13–16]. However, it remains unclear whether cellular recruitment probability across the hippocampal long axis depends on task or is invariant to changes in cognitive-behavioural demands.

To address this question, we quantified cellular recruitment with the IEG *Arc* across the longitudinal axis of CA1 in female and male rats performing the MWT or context fear discrimination (CFD), which are both impaired following hippocampal damage [17–22]. We focused our behavioral measures on the MWT and CFD due to: 1) their popularity as behavioral assays of long-term memory; 2) differences in extra-hippocampal circuit mechanisms that support the expression of spatial and fear memory in the MWT and CFD [23–25]; 3) to extend our previous results on *Arc* mRNA expression in the MWT across sexes [11]. While these tasks may share emotional components during early performance, others have shown that stress responses in the MWT are elevated in early sessions but significantly reduced during later training [26,27]. In addition, our group and others have shown that regions associated with emotional processing such as the basolateral amygdala are not required for the expression of spatial memory in the MWT [28], but are required for CFD [29]. We have also reported that hippocampal damage causes retrograde but not anterograde amnesia in the present CFD task, which uses highly distinct sensory cues [20]. Our CFD paradigm is thus thought to place greater demand on emotional processes than spatial processing due to the lack of anterograde amnestic effects with hippocampal damage and salient, distinct contextual features used. In the present work, we chose to focus on CA1 due its central role in integrating hippocampal computations and operating as a primary "output" to extra-hippocampal structures, and the observation that CA1-restricted damage impairs both the MWT and numerous forms of contextual fear memory [30,31]. We further measured *Arc* mRNA expression as an indicator of population activity due to its established role in LTP, memory retrieval, and relatively precise temporal pattern of expression compared to other IEG transcripts and protein-level expression [32]. *Arc* has been used in numerous studies of cellular recruitment across the hippocampal long axis and thus allows for comparison between our results and previous findings [9–11,33]. Although this approach might also afford some detection of changes in neuronal firing rates during task performance [34], we focus in the present study on recruitment in CA1 as it relates to the proportion of active cells.

With this approach, we designed an experiment to adjudicate between two predicted outcomes of the cognitive function and granular hypotheses on cellular recruitment in dorsal and ventral CA1, respectively: 1) *Arc* expression will be greater in dorsal than ventral CA1 in the MWT due to greater requirements of spatial processing during memory retrieval and, by contrast, greater in ventral than dorsal CA1 during CFD due to greater emotional processing in fear memory retrieval; 2) *Arc* expression will be greater in dorsal than ventral CA1 regardless of the task performed due to differences in the granularity of task representation across the longitudinal axis.

2. Materials and methods

2.1. Subjects

The University of Lethbridge Animal Welfare Committee approved all procedures used in the present experiments, which also meet the Canadian Council of Animal Care guidelines. A total of 24 Long Evans rats weighing between 300 and 350 g were used in the present experiments, including 12 females and 12 males (Charles River, Raleigh, NC). Previous work in our lab and others have determined such group sizes provide adequate statistical power for within-animal and across-group comparisons for behavioural and cellular levels of analysis [9,11,36,37]. Following their arrival at the University of Lethbridge, animals were allowed at least 1 week to acclimatize to colony room conditions and were handled 5 min each day by the experimenter for 5 days before the start of the experiment.

2.2. Experimental design

To match behavioural experience across animals, male and female rats were equally divided into cohorts and trained in the MWT and CFD in counterbalanced order before final testing and perfusion (Fig. 1). Our rationale for training animals both tasks was two-fold: 1) to ensure similar cumulative experience prior to final testing and perfusion that might otherwise affect plasticity and subsequent *Arc* transcription dynamics; 2) to ensure similar performance of groups in MWT and CFD performance. Each animal experienced the MWT and CFD task for 4 days each, with one day of rest between paradigms (Fig. 1E). During training in the MWT, rats were transported from the animal colony to the behavioural testing room in covered cages on a cart. Surrounding the swimming pool were several posters on the walls, a table, and computer rack that served as allocentric cues to help animals navigate. During each session, animals were monitored, and relevant behavioural variables (latency and quadrant dwelling) were calculated using EthoVision XT software (Noldus) from an overhead behavioural camera. The MWT apparatus consisted of a 2-meter diameter pool filled with room temperature water (~25 C) that was made opaque using white non-toxic tempura paint. On days 1–3, rats were given 8 trials (maximum 60 s) starting randomly from one of the four cardinal positions at the edge of the pool to locate a hidden platform approximately 5 cm beneath the water surface located in the center of the Northwest quadrant. If the animal did not locate the hidden platform within 60 s they were placed onto the platform by the experimenter. Animals were then allowed 10 s to remain on the platform before placement back into their holding cage by the experimenter for an approximate 5-minute intertrial interval. Following completion of the 8 swim trials each day, rats were returned to their colony room for approximately 24 h prior to subsequent behavioural training or testing. During the final testing day in the MWT, animals were individually transported in covered cages and given 4 swim trials with a 2-minute intertrial interval for a total 10-minute testing period. Half of the animals from female and male groups were sacrificed and perfused following MWT testing (Fig. 1E).

In the CFD task, rats were individually transported in a covered holding cage by the experimenter to a room with several posters on the walls, a storage shelf, and the CFD apparatus, which consisted of two conditioning chambers (contexts) and connecting alleyway. One context was a black triangle that was 61 cm long, 61 cm wide, and 30 cm high with stainless steel rod flooring, and was scented with banana (Isoamyl Acetate, Sigma) located in a perforated pill bottle at the top right corner of the chamber. The other context was a white square that was 41 cm long, 41 cm wide, and 30 cm high with stainless steel rod flooring and was scented with Eucalyptus (Vic's VapoRub©) located in a perforated pill bottle inserted through the top left corner of the chamber. During each session, animal behaviour was recorded from a tripod-mounted camera from underneath the apparatus through a transparent table. During pre-exposure on day 1 of the CFD task, animals were introduced

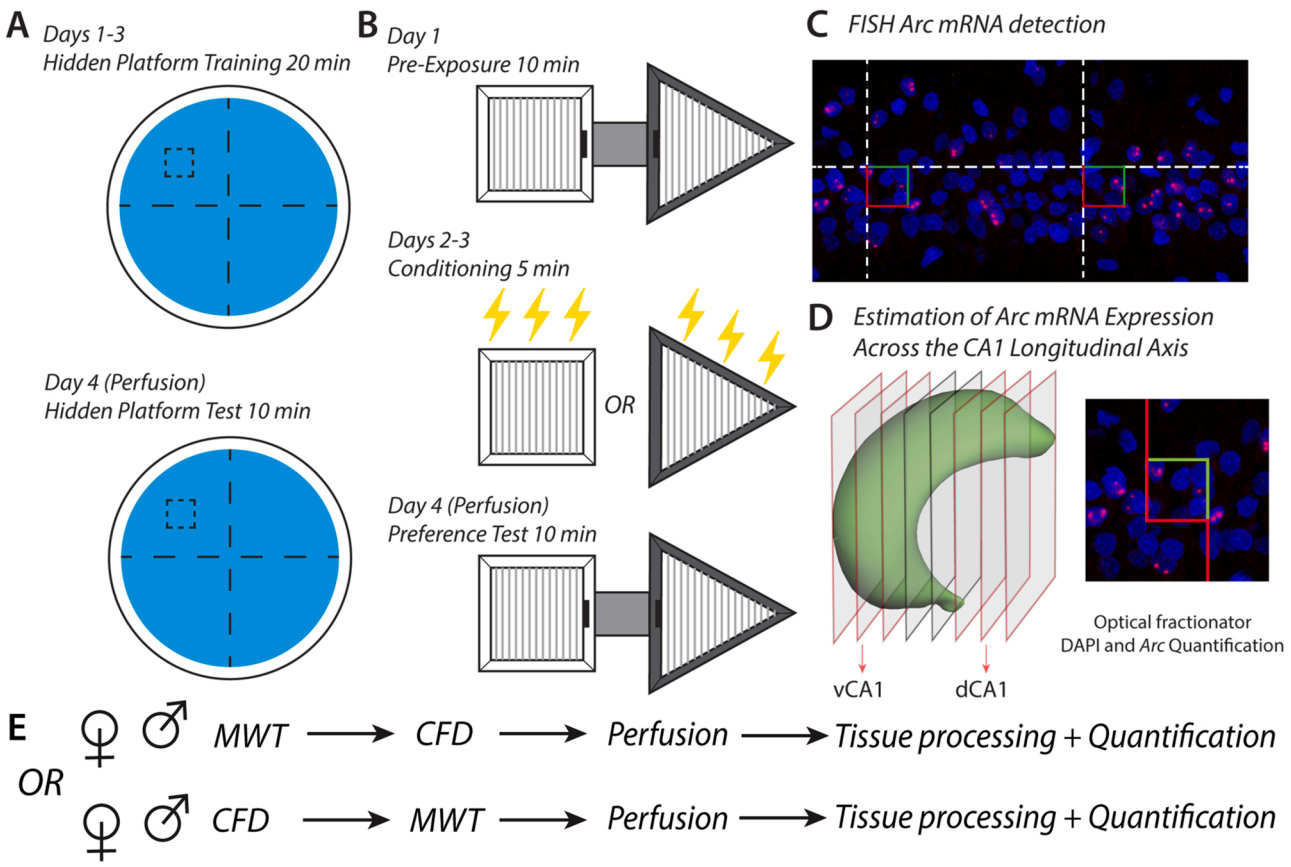

Fig. 1. Experimental design to measure *Arc* mRNA expression across the CA1 long axis during MWT and CFD performance. A) Female and male rats were trained in the MWT using a 4-day procedure, wherein animals learned to swim to locate a hidden platform under the pool surface on days 1–3 and were given a 4-trial test on day 4. Half of the female and male groups were perfused approximately 5–10 min following testing in the MWT. B) Each animal was also trained in CFD, which began with 10 min of pre-exposure to both contexts connected by an alleyway on day 1. Following pre-exposure, animals were conditioned in counterbalanced order to shock-paired and no-shock contexts on days 2–3. Finally, animals were given a 10-minute test to examine preference for the no-shock context and avoidance of shock-paired context on day 4. C) Following testing in the MWT or CFD, animals were perfused, and brains were collected for FISH tissue processing. Brains were then sectioned on a freezing-sliding microtome at 40 μm thickness in a 12-section series, slide mounted, and stained with 4',6'-diamidino-2-phenylindole (DAPI) and digoxygenin-conjugated antisense riboprobes for visualization of nuclear *Arc* mRNA expression (see Methods). A schematic stereological counting grid is overlaid to illustrate the approximate sampling frequency from CA1. D) Following tissue processing, DAPI and *Arc* expression were quantified using the optical fractionator method at 60X magnification on a confocal microscope according to the principles of systematic-random sampling. Estimates from dorsal and ventral CA1 subregions were then divided following quantification across the entire CA1 axis, wherein dorsal CA1 included sections anterior to − 3.8 mm AP from bregma, and ventral sections included sections posterior to − 5.2 mm AP from bregma [35]. E) A schematic illustrates complete experimental design timeline used in the present study.

to the apparatus through the connecting alleyway and allowed to freely explore both contexts for 10 min. On subsequent days 2 and 3, animals were conditioned in shock-paired and no-shock contexts in counter-balanced order. During no-shock conditioning, animals were placed in their no-shock context for 5 min and allowed to explore freely. For shock-paired conditioning, animals were transported to a distinct and separate room containing the same apparatus and placed into their shock-paired context. Shock conditioning was performed in a distinct room with the same apparatus to promote contextual, rather than spatial fear processes (room-based) [25,29,38], due to previous studies that have demonstrated room transfer drives remapping of place cells in CA1 [39]. During shock conditioning, the stainless-steel rod flooring was connected to a Lafayette Instrument Stimtek SGCG1 through a custom shock harness, and 2-second, 1.0 mA scrambled foot shocks were delivered at the 2nd, 3rd, and 4th minute. After an additional 58 s, animals were removed from the shock-paired context and returned to their home cage. On day 4 of the CFD task, animals were returned to the original training room, and introduced to the apparatus through the connecting alleyway and allowed 10 min to explore both contexts. Half of female and male groups were sacrificed and perfused following final preference CFD testing (Fig. 1E). Dwell time in each context was calculated by a trained observer blind to conditions of sex and testing order from video data of the pre-exposure and preference testing epochs and was defined as the presence of both forepaws in a context.

Following final testing in either the MWT or CFD, animals were returned to their holding cage for 1 min, and then given an overdose intraperitoneal injection of sodium pentobarbital. They were then perfused 5–10 min after the completion of behavioural testing in either task, and then decapitated and had their brains extracted for subsequent tissue processing. This timeline was chosen based on previous studies demonstrating that behaviour-driven *Arc* expression is maximal 5–10 min after a learning or remembering episode [40].

2.3. FISH tissue processing

The methods used for *Arc* visualization with FISH are identical to those in our previous report on *Arc* mRNA expression in the MWT [11]. Following fixation and sectioning at 50 μm thickness in a 12-section series using a freezing-sliding microtome, samples were stored at − 80 C until FISH processing. *Arc* riboprobes were designed to detect intronic mRNA sequences, and thus nuclear rather than cytoplasmic expression. Primers flanking *Arc* intron 1, exon 2, and intron 2 were designed using online software (National Center for Biotechnology Information Primer-Blast; credit to A. M. Demchuk, University of

Lethbridge). The exact sequences of the primers and base pair designations follow those of the GenBank accession number NC_005106: 5'-CTTAGAGTTGGGGGAGGGCAGCAG-3' (forward primer, base pairs 2022 - 2045) and 5'-ATTAACCCTCACTAAAGGGCCCTGGGGCCTGTCAGATAGCC-3' (reverse primer tagged with T3 polymerase binding site on 5' end, base pairs 2445–2466). The polymerase chain reaction (PCR) was performed on a genomic rat DNA template using a Taq PCR Kit (New England Biolabs), and the subsequent PCR product was purified using a Qiagen PCR Purification Kit (Life Technologies, Inc.). The MAXIscript T3 transcription kit (Life Technologies, Inc.) and DIG RNA Labeling Mix (Roche Diagnostics) were used to generate DIG-labelled *Arc* intron-specific antisense riboprobes from PCR templates. Riboprobes were then purified with mini QuickSpin columns (Roche Diagnostics), and FISH was performed on slide-mounted tissue as previously described [11,41,42]. Briefly, DIG-labelled *Arc* riboprobe signal was amplified with anti-DIG-POD (1:300; Roche Diagnostics), Tyramide Signal Amplification (TSA) Biotin Tyramide Reagent Pack (1:100; PerkinElmer), and Streptavidin-Texas Red (1:200; PerkinElmer). Cell nuclei were then counterstained with DAPI (1:2000; Sigma-Aldrich).

2.4. Optical fractionator confocal stereology

The approach used for quantification of *Arc* and DAPI labels across the CA1 axis was identical to the methods described in Lee et al. (2019). Briefly, observers blind to experimental conditions of each animal quantified DAPI and *Arc* expression using the optical fractionator method in StereoInvestigator software (version 10.54, MBF Bioscience, VT) from confocal z-stack images collected on an Olympus FV1000 microscope equipped with Fluoview software (version 4.0, Olympus, Shinjuku, Japan). Unilateral traces of CA1 were created at 20X magnification on each section, and counting frames were automatically positioned according systematic-random sampling procedures with a 150 × 150 μm grid over CA1 traces. A series of seven z-stack images at 512 × 512-pixel resolution were collected at each sampling site with a 60X oil-immersion objective starting at the top of the section every 2 μm for a total 14 μm sampling distance in the z-plane. Image thresholds were set at 700 HV ± 20 and 550 HV ± 20, respectively in DAPI and Texas Red channels, and kept constant across imaging each section series such that small *Arc* foci (2–3 pixels in diameter) and DAPI labels could be clearly identified. Digital z-stack images were then imported into StereoInvestigator software, such that the top image from each stack fell above and the final image below a 10-μm height of the optical dissector volume. *Arc* and DAPI were then counted according to optical fractionator inclusion–exclusion criteria at each cell's widest point in a 30 × 30 X 10 μm fractionator probe [43].

2.5. Statistical analysis

Data were analyzed and visualized using the Prism by GraphPad statistical package, in addition to Numpy, Scipy, and Matplotlib libraries with Python 3.7 in Google Colab. A two-way or three-way ANOVA was used to examine main effects and interactions in behavioural and imaging data and post hoc Student's t-test with Šidák correction following a significant interaction term. The variables considered as independent factors in these analyses included sex, quadrant (MWT), context (CFD), epoch, and CA1 subregion (dorsal or ventral). To perform Bayesian analysis, surrogate datasets were generated according to the granular and cognitive hypotheses as described in Results. This analysis and accompanying code can be found in the following Google Colab document: https://colab.research.google.com/drive/1NwdX0rJUXDoX03_krnu6r3BIBtqNZTiR?usp=sharing. Following generation of surrogate data of dorsal and ventral recruitment probability, we calculated the gradient of recruitment as the difference between dorsal and ventral values in simulated data and from actual subjects. Normal distributions were then fit to each gradient in the MWT and CFD, and we calculated the BF as the ratio of the integrated product between the actual data and granular distributions versus cognitive hypothesis in each task. Using this method, we interpreted a BF from 10 to 30 as strong evidence for the granular hypothesis, and a BF score from 1/10–1/30 as strong evidence for the cognitive view.

3. Results

Our behavioural results in the MWT and CFD show clear, successful learning in spatial and fear tasks for both male and female rats under the present training and test protocols. A two-way analysis of variance (ANOVA) of latency to locate the hidden platform in the MWT showed significant effects of day ($F(3,66)= 45.01$, $p < 0.0001$) and sex ($F(3,66)= 5.129$, $p = 0.0337$), but not a significant day x sex interaction ($F(3,66)= 0.08432$, $p = 0.9684$; Fig. 2A), with female rats slower than males to reach the hidden platform. To ensure that the effect of sex on MWT performance was not an artifact of slower swim speed, we also examined the percentage of dwell time in target versus non-target pool quadrants across days (Fig. 2B). A three-way ANOVA revealed day ($F(3,66)= 24.45$, $p < 0.0001$), quadrant ($F(1,22)= 464.9$, $p < 0.0001$), and sex ($F(1,22)= 11.50$, $p = 0.0026$) as significant factors, in addition to significant sex x quadrant ($F(1,22)= 11.50$, $p = 0.0026$) and day x quadrant interactions ($F(3,66)= 24.45$, $p < 0.0001$). Thus, like some previous reports we found that males are somewhat faster and more accurate in allocentrically-based MWT navigation than females [44–47]. Despite effects of sex, post-hoc comparisons between target and non-target quadrants on day 4 showed significant preference for the target quadrant in both male ($t = 17.04$, $p < 0.0001$, DF=176) and female rats ($t = 14.01$, $p < 0.0001$, DF=176), demonstrating robust learning of the allocentric MWT in both males and females. Although we did find sex differences in the MWT, both groups performed similarly in CFD. A two-way ANOVA on total dwell time in shock-paired and no-shock contexts during pre-exposure and preference testing revealed a significant effect of context ($F(1,22)= 4.927$, $p = 0.0371$), epoch ($F(1,22)= 12.63$, $p = 0.0018$), and context x epoch interaction ($F(1,22)= 14.31$, $p = 0.0010$), but no effect of sex ($F(1,22)= 2.639$, $p = 0.1185$), context x sex ($F(1,22)= 0.9049$, $p = 0.3518$), epoch x sex ($F(1,22)= 0.1768$, $p = 0.6782$), or context x epoch x sex interaction ($F(1,22)= 1.059$, $p = 0.3145$). To control for possible differences in time spent dwelling in the connecting alleyway during the preference test, we also examined the percent dwell time in shock-paired and no-shock contexts; excluding time spent in the connecting alleyway. A three-way ANOVA on percent dwell time in CFD showed significant effects of context ($F(1,22)= 7.205$, $p = 0.0135$) and context x epoch interaction ($F(1,22)= 24.47$, $p < 0.0001$), but no effect of epoch ($F(1,22)= 0.9995$, $p = 0.3283$), sex ($F(1,22)= 1.000$, $p = 0.3281$), sex x context ($F(1,22)= 0.4861$, $p = 0.4930$), sex x epoch ($F(1,22)= 1.000$, $p = 0.3281$), or sex x context x epoch interaction ($F(1,22)= 0.6604$, $p = 0.4251$). *Post hoc* comparisons also showed significant preference for the no-shock context during preference testing in both males ($t = 3.824$, $p = 0.0015$, DF=88) and females ($t = 5.854$, $p < 0.0001$, DF=88). As a follow-up analysis to ensure that behavioral performance was comparable across cohorts that performed the tasks in counterbalanced order (MWT then CFD or CFD then MWT), we examined test performance in the MWT and CFD in males and females with cohort considered as a factor (graphs not shown). A three way ANOVA of percent context preference in the CFD task showed an effect of context ($F(1,20)= 20.17$, $p = 0.002$), but no effect of cohort ($F(1,20)= 1.000$, $p = 0.3292$), sex ($F(1,20)= 1.000$, $p = 0.3291$), context x cohort ($F(1,20)= 1.623$, $p = 0.2172$), context x sex ($F(1,20)= 0.8830$, $p = 0.3586$), sex x cohort ($F(1,20)= 1.000$, $p = 0.3293$), or context x cohort x sex interaction ($F(1,20)= 0.1575$, $p = 0.6957$). Similarly, a three-way ANOVA of percent dwell time in target and non-target quadrants in the MWT on test day 4 showed an effect of quadrant ($F(1,20)= 193.2$, $p < 0.001$), but no effect of cohort ($F(1,20)= 0.03282$, $p = 0.8581$), sex ($F(1,20)= 2.252$, $p = 0.1491$), quadrant x cohort ($F(1,20)= 0.03282$, $p = 0.8581$), quadrant x sex ($F(1,$

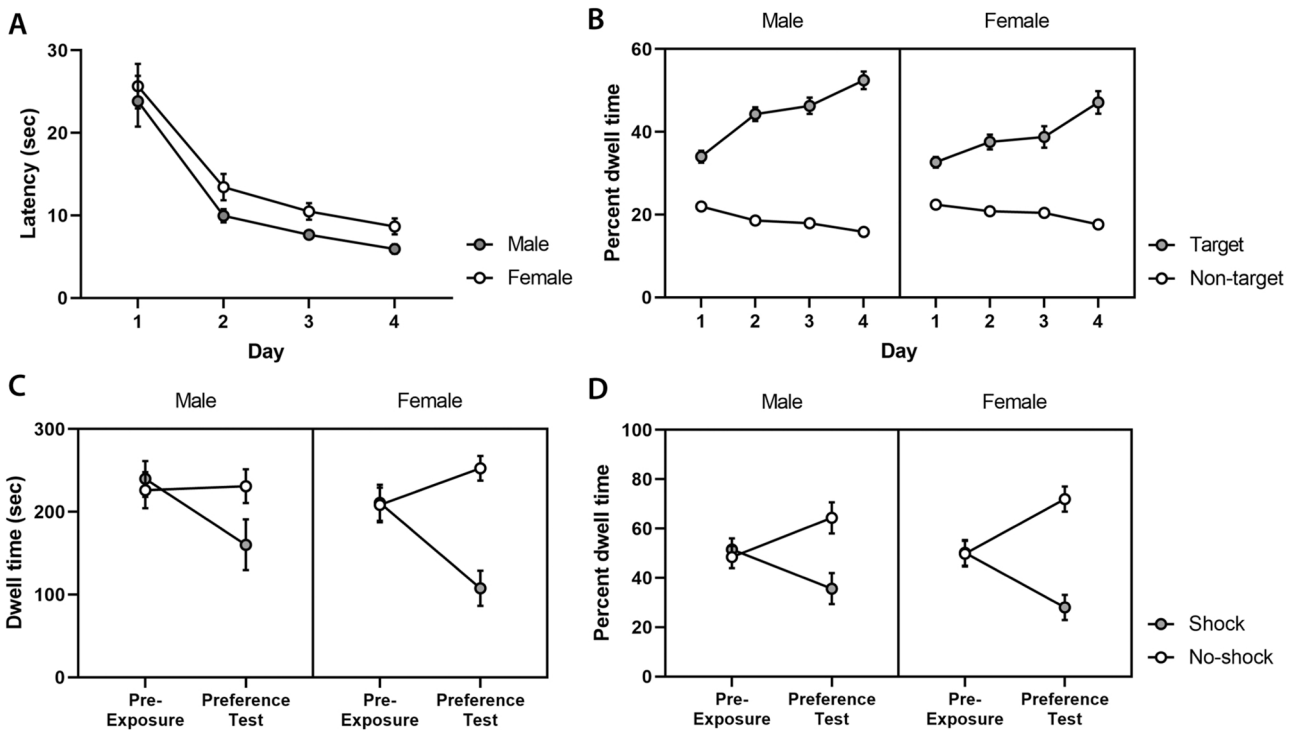

Fig. 2. Female and male behavioural performance in the MWT (A, B) and CFD (C, D). A) Average latency to reach the hidden platform decreased across training (1−3) and test (4) days for both females and males, with males somewhat faster to reach the hidden platform. B) Percent dwell time in target and non-target quadrants showed a strong increase in preference for the target quadrant across training and testing, suggesting that animals effectively learned to navigate to the hidden platform in the MWT. C) Total dwell time in shock-paired and no-shock contexts in the CFD task shows similar preference for both contexts during pre-exposure, and preference for the no-shock context after fear conditioning in female and male animals. D) Controlling for variation in time spent in the connecting alleyway during pre-exposure and preference testing, percent dwell time in shock-paired and no-shock contexts was calculated excluding time spent in the connecting alleyway. Our results demonstrate a similar percent dwell time in the shock-paired and no-shock contexts during pre-exposure, and a strong preference for the no-shock context following conditioning, with no clear effect of sex on CFD performance.

20)= 2.252, $p = 0.1491$), cohort x sex ($F(1,20)= 0.4460$, $p = 0.5119$), or quadrant x cohort x sex interaction ($F(1,20)= 0.4460$, $p = 0.5119$). Finally, a two-way ANOVA of latency to the hidden platform on test day 4 in the MWT showed an effect of sex ($F(1,20)= 5.593$, $p = 0.0283$), but no effect of cohort ($F(1,20)= 0.02483$, $p = 0.8764$) or cohort x sex interaction ($F(1,20)= 0.1504$, $p = 0.7023$). These results thus suggest that both male and female rats expressed robust spatial- and fear-guided behaviour to promote *Arc* expression, and that task order did not significantly affect behavioral performance.

Following behavioural testing in the MWT and CFD, we quantified *Arc* expression using design-based confocal stereology across the entire CA1 longitudinal axis. DAPI-stained cell bodies and *Arc* transcription foci were quantified using the optical fractionator method from confocal z-stacks according to the principles of systematic-random sampling (see Methods for details). We estimated DAPI and *Arc* populations across CA1, including dorsal (anterior to −3.8 mm AP from bregma; Fig. 3A) and ventral (posterior to −5.2 mm from bregma; Fig. 3A) subregions, and transformed these estimates into a single *Arc*:DAPI metric of cellular recruitment probability. A three-way ANOVA of estimated DAPI and *Arc* populations across CA1 (Fig. 3B) showed significant effects of label ($F(1,20)= 1281$, $p < 0.0001$) and sex ($F(1,20)= 7.023$, $p = 0.0154$), but no effect of task ($F(1,20)= 0.08018$, $p = 0.7800$), label x sex ($F(1,20)= 2.203$, $p = 0.1533$), task x sex ($F(1,20)= 0.1407$, $p = 0.7115$), task x label ($F(1,20)= 0.5850$, $p = 0.4533$), or task x sex x label interaction ($F(1,20)= 0.7562$, $p = 0.3948$). Notably, our DAPI estimates closely resemble previous reports of cell number across CA1 (mean DAPI = 418313) using a design-based stereological approach [11,48]. Following transformation of population estimates into *Arc*:DAPI recruitment probability, a two-way ANOVA showed no effect of task ($F(1,20)= 0.08314$, $p = 0.3727$), sex ($F(1,20)= 3.083$, $p = 0.0944$), or task x sex interaction ($F(1,20)= 0.7737$, $p = 0.3895$) on recruitment probability when the entire CA1 population was considered (mean male=0.1728; mean female=0.2021; Fig. 3C). Notably, the magnitude of *Arc* expression observed in CA1 was comparable to levels reported in several studies of open field navigation and dry-land memory tasks, and well above levels observed in home-cage control animals, which is typically between.04 − 0.08 proportion of cells across studies in dorsal and ventral CA1 [10,33,37]. Such levels of home cage activation have been reliably reported across research groups with different quantification methods, and strongly support that the levels of cellular recruitment in the present study are behaviourally-driven [9,10,33,37,49]. To address whether cellular recruitment differs across axis, task, or sex, estimates were divided into dorsal and ventral CA1 *Arc*:DAPI recruitment probabilities (Fig. 3D). A three-way ANOVA showed a significant effect of axis ($F(1,20)= 77.35$, $p < 0.0001$), but no effect of task ($F(1,20)= 0.2344$, $p = 0.6335$), sex ($F(1,20)= 1.772$, $p = 0.1981$), axis x task ($F(1,20)= 0.03415$, $p = 0.8553$), sex x task ($F(1,20)= 0.2616$, $p = 0.6146$), axis x sex ($F(1,20)= 0.3346$, $p = 0.5694$), or axis x task x sex interaction ($F(1,20)= 0.3325$, $p = 0.5706$). Our results thus do not support the cellular recruitment interpretation of the cognitive hypothesis across the CA1 longitudinal axis.

The cognitive and granular accounts of cellular recruitment make distinct predictions about the gradient of *Arc* expression across the CA1 long axis in the MWT and CFD. Namely, the cellular recruitment interpretation of the cognitive hypothesis considered in the present work predicts opposite gradients of cellular recruitment in the two tasks, and the granular model predicts the same gradient across tasks. Importantly, we anticipate opposite outcomes in the CFD task according to each hypothesis, but the same outcome in the MWT. While the above analysis rejects the cognitive account of long axis cellular recruitment, we aimed

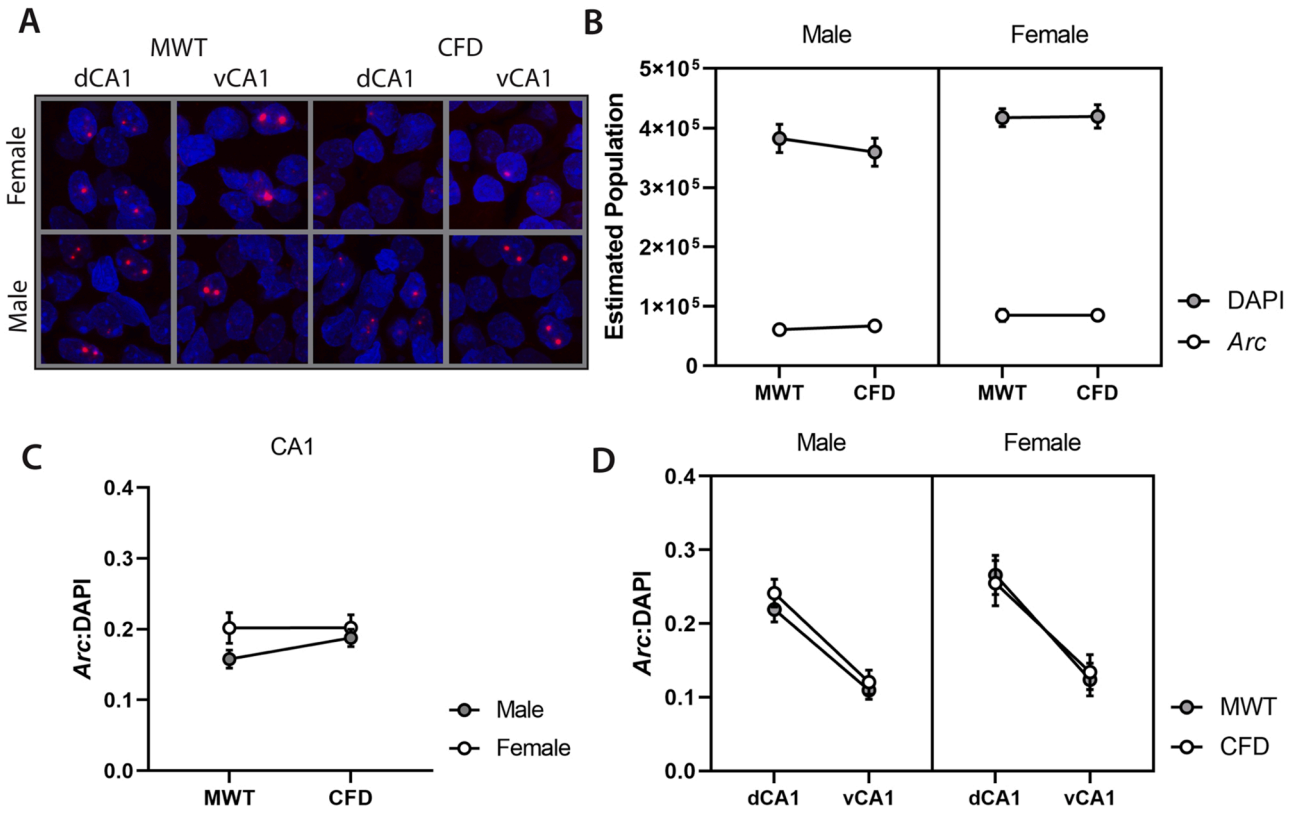

Fig. 3. Quantification of DAPI and *Arc* across the CA1 longitudinal axis in male and female rats performing the MWT and CFD. A) Randomly chosen example images of DAPI and *Arc* labelling in dorsal and ventral CA1 in male and female animals that performed the MWT or CFD. B) Estimated populations of DAPI and *Arc* across CA1 in males and females were similar previous studies using design-based stereology in the rat hippocampus [11,48]. C) Following estimation of DAPI and *Arc* populations, estimates were transformed into *Arc*:DAPI recruitment probabilities for the entire CA1 population. We did not find any differences between males and females in the MWT or CFD *Arc*:DAPI recruitment probabilities when examining the entire CA1 population. D) *Arc*:DAPI recruitment probabilities were then divided into dorsal and ventral CA1 estimates for males and females performing the water task to examine evidence for the granular and cognitive hypotheses. These results show a clear effect of axis in males and females performing both the MWT and CFD, wherein dorsal CA1 has greater recruitment probability than ventral CA1 regardless of task or sex differences.

to directly compare evidence for each view using a Bayesian approach [50]. To this end, we generated surrogate data resembling CA1 estimates of cellular recruitment in each task according the granular and cognitive hypotheses from beta probability distributions, wherein the parameters α and β determine the location and spread of the probability distribution ranging between 0 and 1. The granular model is described by a decaying beta probability distribution ventrally between $\alpha = [5.00, 1.00]$ and $\beta = [10.00, 12.00]$, and the cognitive model is a task-dependent beta probability distribution from $\alpha = [5.00, 1.00]$ and $\beta = [10.00, 12.00]$ in the MWT, and the opposite gradient between $\alpha = [1.00, 5.00]$ and $\beta = [12.00, 10.00]$ in CFD. In addition, we approximated cellular recruitment of home cage controls in our model based on previous reports from several labs that found a similar level of recruitment across dorsal and ventral CA1 [10,33,37,49], with model parameters set to $\alpha = [1.00]$ and $\beta = [15.00]$ for both dorsal and ventral CA1, which yielded an average recruitment of approximately 0.05. Importantly, we estimated these outcomes based on results from several groups to represent variation in observed home cage activity across the CA1 long axis reported in multiple studies [10,37,40]. Further, we chose to estimate these results from previous studies rather than repeat these experiments given the number of times such results have already been reported, which we argue precluded the utility of further animal use to these ends. We then computed the average dorsal and ventral recruitment probabilities from each model and determined the task-dependent recruitment gradient as the difference between dorsal and ventral recruitment in our *Arc*:DAPI dataset and surrogate data (Fig. 4A). Finally, we fit a gaussian likelihood distribution to each dorsal-ventral gradient and computed the Bayes Factor (BF) as the ratio of the integrated product of the actual data from both experimental groups versus the distribution of surrogate home cage data to compute a task-related BF. We then calculated BF for hippocampal long axis models in both tasks from the integrated product of the actual and granular likelihood distributions, versus the actual data and the cognitive likelihood distributions (Fig. 4C). This provides a single BF that describes the ratio of fit between the actual data and each hypothesized distribution, wherein a BF between 10 and 30 was considered as strong evidence for and the granular recruitment hypothesis, and a BF between 1/10 and 1/30 as strong evidence for the cognitive recruitment view. Based on the hypotheses addressed in the current study, alternative parameter assumptions of these models might affect the variation but not the direction of our effects. In comparison to home cage surrogate data (Fig. 4B), BF above 10 or below 1/10 is considered strong evidence for a task-related cellular recruitment gradient. Using this approach, we found strong evidence for a task-related gradient (BF = 13.68), suggesting that the pattern of CA1 recruitment we observed is not explained from results expected in home cage control animals. Comparing models of hippocampal long axis function, we found similar evidence for both hypotheses in the MWT (BF = 1.07; Fig. 4C), and strong evidence for the granular hypothesis in CFD where the predictions of each account differ (BF = 23.09; Fig. 4C). The combined results of these analyses thus favor the granular account to explain variation in cellular recruitment across the CA1 long axis.

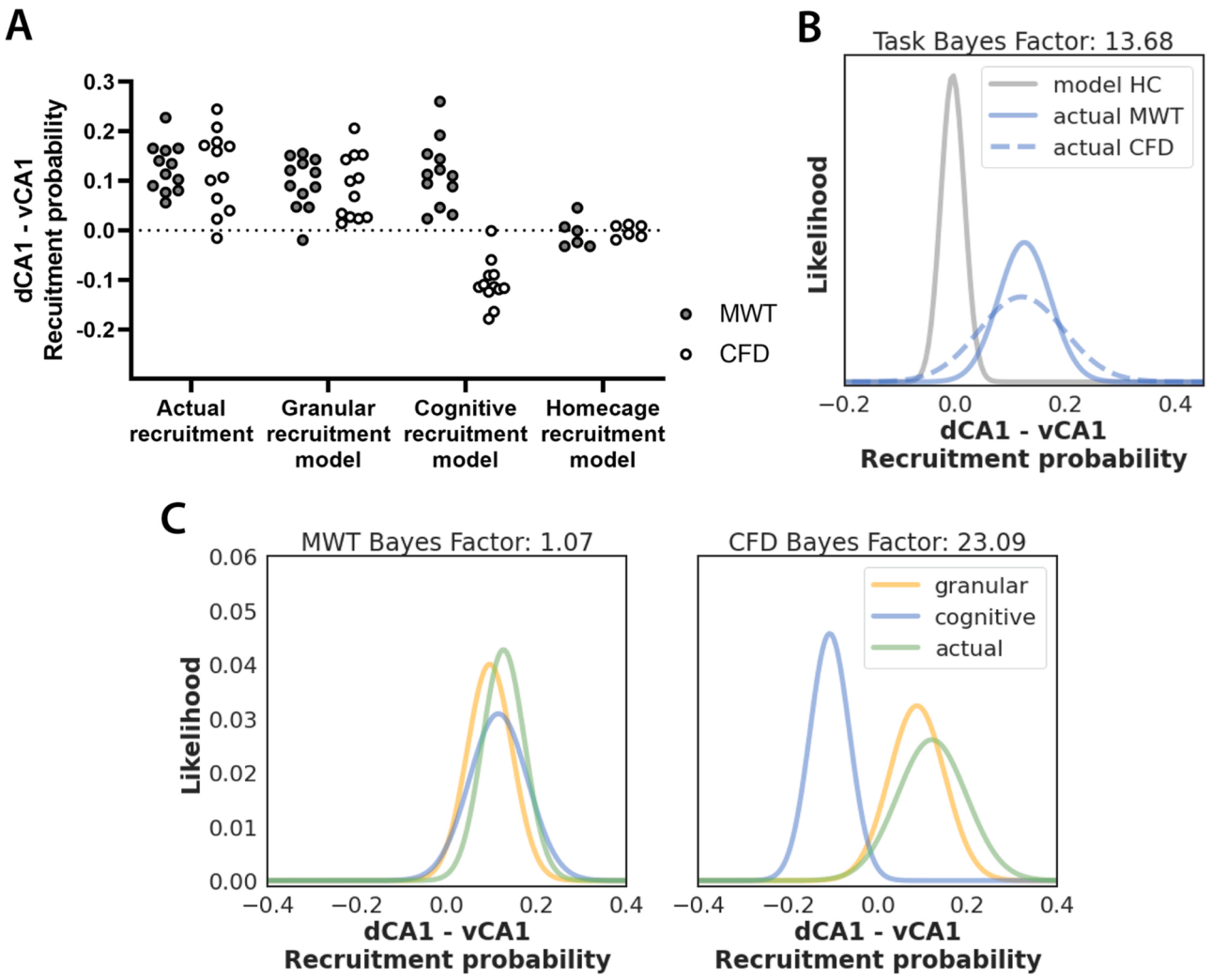

Fig. 4. Bayesian analysis of differential CA1 recruitment probability across the hippocampal long axis in the MWT and CFD. A) Female and male data were combined from the MWT and CFD and the gradient of recruitment probability was calculated as the difference between dorsal and ventral CA1 *Arc*:DAPI estimates. Surrogate data were generated according to home cage control observations in previous studies [9,10,33,37], and the granular and cognitive hypotheses of dorsal and ventral CA1 cellular recruitment. We then computed the difference between dorsal and ventral estimates from surrogate and actual data in the MWT and CFD to generate model-based recruitment probability gradients. B) Normal distributions were fit to actual and surrogate home cage data to compute a task-related BF as the ratio of the integrated product of actual distributions compared to the home cage control distribution, which demonstrated the gradient of cellular recruitment we observed is behaviourally driven. C) Normal distributions were also fit to surrogate and actual dataset from the MWT and CFD, and the BF was computed as the ratio between the integrated products of the actual and surrogate distributions according to the granular versus the cognitive hypothesis. Using this approach, we observed greater evidence for the granular view of the hippocampal long axis function to describe cellular recruitment probabilities.

4. Discussion

In the present experiment, we have found that cellular recruitment probability is greater in dorsal than ventral CA1 during performance of the MWT and CFD in both male and female rats. While previous work has demonstrated the same effect in using the IEG *Arc* during open-field navigation and memory retrieval [9,10], our results are the first to demonstrate such a gradient of activity across the hippocampal long axis in a fear-based task. Further, the present findings replicate our previous result that cellular recruitment is greater in dorsal than ventral CA1 during navigation in the MWT [11], and bear great similarity to the pattern of recruitment in tasks that have no clear aversive component [9,10,33]. While we cannot rule out that some level of cellular recruitment could be driven by aversive components in both MWT and CFD tasks, the semblance of our findings to previous open-field studies and appetitive tasks suggests that emotion is not a strong contributor to the size of recruited populations across the CA1 long axis. These findings across several studies and research groups suggest that the dorsal-ventral gradient of recruitment in CA1 may be an invariant property of this region. Our results are also the first to our knowledge that demonstrate such recruitment dynamics are shared across sexes. Despite differences in performance between males and females in the MWT, we did not find differences in their pattern cellular recruitment. Finally, our analysis comparing these results against the cellular recruitment interpretation of the granular and cognitive hypotheses support the granular view on hippocampal long axis function (Fig. 4). Future work should examine how such gradients might also differ across additional hippocampal subregions, including the dentate gyrus (DG), CA3, and the subiculum. If the granularity hypothesis explains recruitment dynamics across all subregions, we anticipate the same gradient of cellular recruitment in the MWT and CFD, with inter-regional differences in overall levels of activation, with the DG, CA3, CA1, and subiculum showing increasing levels of recruitment, respectively, like previous open-field studies [9,10,51].

Notably, one benefit of the CFD paradigm to assay cellular recruitment across the hippocampal long axis is that *Arc* expression is likely to

be driven more robustly in the hippocampus when animals are engaged in active movement (avoidance of a shock-paired context) compared to a freezing behavior that is measure in classical context or tone fear conditioning paradigms, which produces lower levels of neuronal activity [52,53]. Although animals received shock-paired conditioning in a separate room from final testing, it remains possible that the CFD paradigm engaged more spatial processing than other fear tasks such as classical tone fear conditioning. Additionally, while we have trained animals for multiple days in the MWT to reduce stress levels upon final testing, this task is more aversive in comparison to reward-based, dry-land navigation tasks. Future experiments might examine cellular recruitment across in CA1 while animals perform tone-fear and dry-land navigation tasks. If the granularity view correctly explains variation in cellular recruitment across the hippocampal long axis regardless of the task performed, then we predict the same pattern of results as observed here.

Evidence from lesion, electrophysiological, functional imaging, and IEG studies supports that the hippocampus functionally differs across its longitudinal axis [1,4,5,9,18]. While arguments have been made from these observations in support of either a cognitive or granular account of this difference, the present results in CA1 lend greater support to the granular hypothesis specifically to explain cellular recruitment dynamics. Several observations from navigation, memory, and cognitive mapping literature inform this view. Of these findings, perhaps the most characterized is the gradient in place field size that increases across the hippocampal long axis ventrally. Several groups have found that while average place field diameter is often < 1 m in dorsal hippocampal regions, field diameter in the ventral pole can range up to 10 m [8]. In keeping with this observation, recent comparisons of dorsal and ventral hippocampal lesions in the MWT have shown that while dorsal lesions impair precise localization of goal locations, ventral damage impairs coarse localization in the MWT [17–19]. In relation to cellular recruitment, it is anticipated that cells in the dorsal hippocampus are more likely to be recruited due to a greater number of small place fields that might be required to tessellate a space than those with large fields in ventral hippocampus [6,7]. Indeed, multiple groups have found that place cells in the dorsal hippocampus have multiple fields in large environments [54–58]. Recently, Harland et al. [59] also reported that place cells recorded in the dorsal hippocampus during navigation in a two-dimensional "megaspace" ($>18\ m^2$) express multiple fields of varying sizes that tend to increase with scale of the environment, and recently the same finding was reported in bats [58]. They also found a negative correlation between field number and average field size, suggesting that perhaps the granularity of representation might be related to the recruitment probability. However, the relationship between place field size and recruitment probability across the hippocampal long axis is not well understood. Future experiments to evaluate the granularity view might consider manipulations of room size or spatial sampling during open field navigation as in Witharana et al. [51] and measuring cellular recruitment across the hippocampal long axis. Despite the present support from these experiments for the granular view of the hippocampal longitudinal axis, it is also important to consider evidence that favours the cognitive view.

The cognitive function view stems from considering anatomical projections and functional cell types that differ in dorsal and ventral regions. While dorsal CA1 and subiculum have strong efferent projection to the retrosplenial, rhinal, and post-rhinal cortices, ventral CA1 and subiculum project to the rhinal and medial prefrontal cortices (mPFC), basal and central amygdala, ventral striatum, and lateral hypothalamus [1,4,52]. As a result, information represented across the hippocampal long axis projects to distinct targets and receives input from many of these regions. Previous reports have shown that synchronized activity between the ventral hippocampus and mPFC modulates anxiety behaviour [60], and recent calcium imaging experiments have also revealed functional cell types that respond to shock and anxiety in ventral hippocampus that project monosynaptically to the basal amygdala and lateral hypothalamus, respectively [52,61]. However, despite the presence of anxiety and shock-responsive cells in ventral hippocampus, recent studies also point to the existence of shock-responsive cells in dorsal CA1 [53,62]. Further, several groups have found that many cells in dorsal CA1 are responsive to reward [56,63–66], and optogenetic activation of such cells results in reward-seeking behaviour [64]. While some studies have reported differential impairments of dorsal and ventral hippocampal lesions in tasks that require emotional regulation, such as contextual fear conditioning, some also demonstrate that dorsal and ventral lesions similarly impair performance in such tasks, including non-spatial delay tone conditioning [2,67–69]. Indeed, our group and others have also shown that CFD is impaired following either dorsal, ventral, or complete hippocampal damage [17,20,70,71]. While some evidence supports that behavioural variables are differently coded across the hippocampal long axis, the causal relationship between dorsal and ventral regions with spatial and emotional behaviour may not be mutually exclusive.

In the present experiments, we have chosen to focus our analysis on binary cellular recruitment dynamics (proportions of active cells) but have not examined potential task-driven variation in neuronal firing rate across the CA1 long axis. Importantly, recent neurophysiological experiments supporting the cognitive hypothesis have focused primarily on firing rate differences across the hippocampal long axis during task performance [52,61]. Another interpretation of the cognitive function view of the hippocampal long axis not examined here is that cognitive demands will drive changes in cellular firing rate, and not the size of recruited neuronal population. The cognitive view may not explain cellular recruitment dynamics across the hippocampal long axis, but instead changes specifically in neuronal firing rate; this interesting possibility should be examined in parallel with recruitment dynamics in future studies. Specifically, what is the relationship between cellular recruitment and firing rates across behavioral states? Such statistical description of neuronal dynamics will help to refine theoretical heuristics on functional differences across the hippocampal axes.

Another possible explanation of differences that we have observed in *Arc* expression across the CA1 longitudinal axis could be related to cellular excitability and intrinsic recruitment propensity. In dorsal CA1, several studies have reported that cellular recruitment does not follow a Poisson process (random draw with replacement), but instead is gamma or log-normally distributed [51,56,57]. Recently, Lee et al. (2020) found that most cells in CA1 are virtually "silent" and have no place fields across multiple, large environments, while some cells have single fields, and a minority of cells have multiple fields in multiple environments – in keeping with recruitment statistics of hippocampal cells in multi-room IEG studies [51]. Importantly, Lee et al. [56] also found that cellular excitability is positively related to the propensity of cells to express fields for multiple places, environments, rewards, and across time. Cellular excitability and resultant propensity likely have a direct role in cellular recruitment probability and coding sparsity. While previous whole-cell patch recordings have revealed that ventral CA1 neurons are more intrinsically excitable than in dorsal CA1 [72,73], it remains unclear whether the excitability-propensity relationship is constant across the hippocampal long axis, and whether propensity-based recruitment distributions are similar or differ. Based on the present results and previous studies of cellular recruitment [9,11,51], we anticipate fewer overall cells to have fields in ventral than dorsal CA1 possibly due to differences in afferent projection and less dendritic length and surface area in ventral CA1 [72]. However, those cells with the propensity to have fields would be more excitable in ventral than dorsal CA1. This would suggest that the gamma-distributed process of recruitment differs across the hippocampal long axis, although this has not been examined experimentally. Indeed, variation in propensity across the long axis might impose biophysical constraints in the hippocampal system that produce differences in function across the hippocampal long axis, perhaps in keeping with the cognitive and/or granular view. Future work might therefore explore the relationship between excitability,

propensity, and cellular recruitment across the hippocampal longitudinal axis, and its potential role in determining the nature of hippocampal representation and encoding of behavioural variables.

Funding

This research was supported by Natural Sciences and Engineering Research Council of Canada (NSERC) Discovery Grants awarded to RJM (DG 06347) and RJS (DG 8318).

CRediT authorship contribution statement

J. Quinn Lee: Conceptualization, Methodology, Software, Formal analysis, Validation, Data curation, Writing – original draft, Writing – review and editing, Visualization, Supervision. **Rebecca McHugh**: Methodology, Data curation, Investigation, Writing – review and editing. **Erik Morgan**: Methodology, Data curation, Investigation. **Robert J. Sutherland**: Methodology, Supervision, Writing – review and editing, Funding acquisition. **Robert J. McDonald**: Conceptualization, Methodology, Supervision, Writing – original draft, Writing – review and editing, Project administration, Funding acquisition.

Declaration of Competing Interest

None.

Acknowledgements

We thank Valérie Lapointe, Aubrey Demchuk, Nhung Hong, and Maurice Needham for their assistance with this project.

References

[1] B.A. Strange, et al., Functional organization of the hippocampal longitudinal axis, Nat. Rev. Neurosci. 15 (10) (2014) 655–669.
[2] D.M. Bannerman, et al., Regional dissociations within the hippocampus—memory and anxiety, Neurosci. Biobehav. Rev. 28 (3) (2004) 273–283.
[3] M.B. Moser, E. Moser, Functional differentiation in the Hippocampus, Hippocampus 8 (1998) 608–619.
[4] M.S. Fanselow, H.-W. Dong, Are the dorsal and ventral hippocampus functionally distinct structures? Neuron 65 (1) (2010) 7–19.
[5] M. Jung, S. Wiener, B. McNaughton, Comparison of spatial firing characteristics of units in dorsal and ventral hippocampus of the rat, J. Neurosci. 14 (12) (1994) 7347–7356.
[6] A.P. Maurer, et al., Self-motion and the origin of differential spatial scaling along the septo-temporal axis of the hippocampus, Hippocampus 15 (7) (2005) 841–852.
[7] A.P. Maurer, L. Nadel, The continuity of context: a role for the hippocampus, Trends Cogn. Sci. 25 (3) (2021) 187–199.
[8] K.B. Kjelstrup, et al., Finite scale of spatial representation in the hippocampus, Science 321 (5885) (2008) 140–143.
[9] M.K. Chawla, et al., Behavior-driven arc expression is reduced in all ventral hippocampal subfields compared to CA1, CA3, and dentate gyrus in rat dorsal hippocampus, Hippocampus 28 (2018) 178–185.
[10] Z. Beer, C. Chwiesko, M.M. Sauvage, Processing of spatial and non-spatial information reveals functional homogeneity along the dorso-ventral axis of CA3, but not CA1, Neurobiol. Learn. Mem. 111 (2014) 56–64.
[11] J.Q. Lee, et al., Place navigation in the Morris water task results in greater nuclear Arc mRNA expression in dorsal compared to ventral CA1, Hippocampus 29 (11) (2019) 1133–1138.
[12] S.D. Vann, et al., Fos imaging reveals differential patterns of hippocampal and parahippocampal subfield activation in rats in response to different spatial memory tests, J. Neurosci. 20 (7) (2000) 2711–2718.
[13] N.C. Huff, Amygdala regulation of immediate-early gene expression in the hippocampus induced by contextual fear conditioning, J. Neurosci. 26 (5) (2006) 1616–1623.
[14] J. Czerniawski, et al., The importance of having arc: expression of the immediate-early gene arc is required for hippocampus-dependent fear conditioning and blocked by NMDA receptor antagonism, J. Neurosci. 31 (31) (2011) 11200–11207.
[15] M. Zelikowsky, et al., Neuronal ensembles in amygdala, hippocampus, and prefrontal cortex track differential components of contextual fear, J. Neurosci. 34 (25) (2014) 8462–8466.
[16] N.A. Heroux, et al., Medial prefrontal and ventral hippocampal contributions to incidental context learning and memory in adolescent rats, Neurobiol. Learn. Mem. 166 (2019), 107091.
[17] R.J. McDonald, et al., Rats with ventral hippocampal damage are impaired at various forms of learning including conditioned inhibition, spatial navigation, and discriminative fear conditioning to similar contexts, Behav. Brain Res. 351 (2018) 138–151.
[18] S. Ruediger, et al., Goal-oriented searching mediated by ventral hippocampus early in trial-and-error learning, Nat. Neurosci. 15 (11) (2012) 1563–1571.
[19] J. Ferbinteanu, C. Ray, R.J. McDonald, Both dorsal and ventral hippocampus contribute to spatial learning in Long–Evans rats, Neurosci. Lett. 345 (2) (2003) 131–135.
[20] J.Q. Lee, R.J. Sutherland, R.J. McDonald, Hippocampal damage causes retrograde but not anterograde memory loss for context fear discrimination in rats, Hippocampus 27 (9) (2017) 951–958.
[21] R.G.M. Morris, et al., Place navigation impaired in rats with hippocampal lesions, Nature 297 (5868) (1982) 681–683.
[22] R.J. Sutherland, B. Kolb, I.Q. Whishaw, Spatial mapping: definitive disruption by hippocampal or medial frontal cortical damage in the rat, Neurosci. Lett. 31 (3) (1982) 271–276.
[23] J.R. Whitlock, et al., Navigating from hippocampus to parietal cortex, Proc. Natl. Acad. Sci. 105 (39) (2008) 14755–14762.
[24] R.R. Rozeske, C. Herry, Neuronal coding mechanisms mediating fear behavior, Curr. Opin. Neurobiol. 52 (2018) 60–64.
[25] R.J. McDonald, N.S. Hong, How does a specific learning and memory system in the mammalian brain gain control of behavior? Hippocampus 23 (11) (2013) 1084–1102.
[26] A. Aguilar-Valles, et al., Analysis of the stress response in rats trained in the water-maze: Differential expressoin of corticotropin-releasing hormone, CRH-R1, glucocorticoid receptors and brain-derived neurotrophic factor in limbic regions, Neuroendocrinology 82 (2006) 306–319.
[27] K. Bromley-Brits, Y. Deng, W. Song, Morris water maze test for learning and memory deficits in Alzheimer's disease model mice, J. Vis. Exp. (53) (2011).
[28] R.J. McDonald, et al., Expression of a conditioned place preference or spatial navigation task following muscimol-induced inactivations of the amygdala or dorsal hippocampus: a double dissociation in the retrograde direction, Brain Res. Bull. 83 (1–2) (2010) 29–37.
[29] E. Antoniadis, Amygdala, hippocampus and discriminative fear conditioning to context, Behav. Brain Res. 108 (1) (2000) 1–19.
[30] A.C. Ocampo, L.R. Squire, R.E. Clark, Hippocampal area CA1 and remote memory in rats, Learn. Mem. 24 (11) (2017) 563–568.
[31] A.C. Ocampo, L.R. Squire, R.E. Clark, The beneficial effect of prior experience on the acquisition of spatial memory in rats with CA1, but not large hippocampal lesions: a possible role for schema formation, Learn. Mem. 25 (3) (2018) 115–121.
[32] O. Steward, P.F. Worley, A cellular mechanism for targeting newly synthesized mRNAs to synaptic sites on dendrites, Proc. Natl. Acad. Sci. 98 (13) (2001) 7062–7068.
[33] B. Schmidt, et al., Cognitive demands induce selective hippocampal reorganization: arcexpression in a place and response task, Hippocampus 22 (11) (2012) 2114–2126.
[34] W.K.L. Witharana, et al., Immediate-early gene Homer1a intranuclear transcription focus intensity as a measure of relative neural activation, Hippocampus 29 (6) (2019) 481–490.
[35] G. Paxinos, C. Watson. The Rat Brain in Stereotaxic Coordinates, 7th edition ed.,, Academic Press, 2013.
[36] J.Q. Lee, et al., Relocating cued goals induces population remapping in CA1 related to memory performance in a two-platform water task in rats, Hippocampus 28 (2018) 431–440.
[37] J.F. Guzowski, et al., Environment-specific expression of the immediate-early gene Arc in hippocampal neuronal ensembles, Nat. Neurosci. 2 (12) (1999) 1120–1124.
[38] R.J. McDonald, N.S. Hong, The Wiley-Blackwell Handbook on the Cognitive Neuroscience of Learning, in: R.A. Murphy, R.C. Honey (Eds.), Mechanisms of contextual conditioning, Wiley, 2016.
[39] L.L. Colgin, E.I. Moser, M.-B. Moser, Understanding memory through hippocampal remapping, Trends Neurosci. 31 (9) (2008) 469–477.
[40] J.F. Guzowski, et al., Imaging neural activity with temporal and cellular resolution using FISH, Curr. Opin. Neurobiol. 11 (5) (2001) 579–584.
[41] C.J. Montes-Rodríguez, et al., Postnatal development ofHomer1ain the rat hippocampus, Hippocampus 23 (10) (2013) 890–902.
[42] D.F. Marrone, et al., Immediate-early gene expression at rest recapitulates recent experience, J. Neurosci. 28 (5) (2008) 1030–1033.
[43] C. Schmitz, P.R. Hof, Design-based stereology in neuroscience, Neuroscience 130 (4) (2005) 813–831.
[44] R.S. Astur, M.L. Ortiz, R.J. Sutherland, A characterization of performance by men and women in a virtual Morris water task, Behav. Brain Res. 93 (1–2) (1998) 185–190.
[45] J. Faraji, G.A. Metz, R.J. Sutherland, Characterization of spatial performance in male and female Long-Evans rats by means of the Morris water task and the ziggurat task, Brain Res. Bull. 81 (1) (2010) 164–172.
[46] R.J. Keeley, et al., Sex difference in cue strategy in a modified version of the morris water task: correlations between brain and behaviour, PLoS ONE 8 (7) (2013), e69727.
[47] T.S. Perrot-Sinal, et al., Sex differences in performance in the Morris water maze and the effects of initial nonstationary hidden platform training, Behav. Neurosci. 110 (6) (1996) 1309–1320.
[48] I. Heggland, et al., Stereological estimation of neuron number and plaque load in the hippocampal region of a transgenic rat model of Alzheimer's disease, Eur. J. Neurosci. 41 (9) (2015) 1245–1262.
[49] J.F. Guzowski, et al., Experience-dependent gene expression in the rat hippocampus after spatial learning: a comparison of the immediate-early GenesArc, c-fos, andzif268, J. Neurosci. 21 (14) (2001) 5089–5098.

[50] C.R. Gallistel, The importance of proving the null, Psychol. Rev. 116 (2) (2009) 439–453.
[51] W.K.L. Witharana, et al., Nonuniform allocation of hippocampal neurons to place fields across all hippocampal subfields, Hippocampus 26 (10) (2016) 1328–1344.
[52] S. Ciocchi, et al., Selective information routing by ventral hippocampal CA1 projection neurons, Science 348 (6234) (2015) 560–563.
[53] P.J. Schuette, et al., Long-term characterization of hippocampal remapping during contextual fear acquisition and extinction, J. Neurosci. 40 (43) (2020) 8329–8342.
[54] A.A. Fenton, et al., Unmasking the CA1 ensemble place code by exposures to small and large environments: more place cells and multiple, irregularly arranged, and expanded place fields in the larger space, J. Neurosci. 28 (44) (2008) 11250–11262.
[55] B.C. Harland, et al., Dorsal CA1 Hippocampal Place Cells Form a Multi-Scale Representation of Megaspace, Cold Spring Harbor Laboratory, 2021.
[56] J.S. Lee, et al., The statistical structure of the hippocampal code for space as a function of time, context, and value, Cell 183 (3) (2020) 620–635.e22.
[57] P.D. Rich, H.P. Liaw, A.K. Lee, Large environments reveal the statistical structure governing hippocampal representations, Science 345 (6198) (2014) 814–817.
[58] T. Eliav, et al., Multiscale representation of very large environments in the hippocampus of flying bats, Science 372 (6545) (2021) eabg4020.
[59] B.C. Harland, et al., Dorsal CA1 hippocampal place cells form a multi-scale representation of megaspace, Curr. Biol. 31 (10) (2021) 2178–2190.
[60] A. Adhikari, M.A. Topiwala, J.A. Gordon, Synchronized activity between the ventral hippocampus and the medial prefrontal cortex during anxiety, Neuron 65 (2) (2010) 257–269.
[61] J.C. Jimenez, et al., Contextual fear memory retrieval by correlated ensembles of ventral CA1 neurons, Nat. Commun. 11 (1) (2020).
[62] R.R. Rozeske, et al., Examination of non-spatially tuned hippocampal neurons in a context fear discrimination task, Soc. Neurosci. (2019).
[63] J.L. Gauthier, D.W. Tank, A dedicated population for reward coding in the hippocampus, Neuron 99 (1) (2018) 179–193.e7.
[64] N.T.M. Robinson, et al., Targeted activation of hippocampal place cells drives memory-guided spatial behavior, Cell 183 (7) (2020) 2041–2042.
[65] V. Hok, et al., Goal-related activity in hippocampal place cells, J. Neurosci. 27 (3) (2007) 472–482.
[66] G.P. Gava, et al., Integrating new memories into the hippocampal network activity space, Nat. Neurosci. 24 (3) (2021) 326–330.
[67] D.M. Bannerman, et al., Double dissociation of function within the hippocampus: a comparison of dorsal, ventral, and complete hippocampal cytotoxic lesions, Behav. Neurosci. 113 (6) (1999) 1170–1188.
[68] N.J. Broadbent, R.E. Clark, Remote context fear conditioning remains hippocampus-dependent irrespective of training protocol, training–surgery interval, lesion size, and lesion method, Neurobiol. Learn. Mem. 106 (2013) 300–308.
[69] R.J. Sutherland, J. O'Brien, H. Lehmann, Absence of systems consolidation of fear memories after dorsal, ventral, or complete hippocampal damage, Hippocampus 18 (7) (2008) 710–718.
[70] D.C. Gidyk, R.J. McDonald, R.J. Sutherland, Intact behavioral expression of contextual fear, context discrimination, and object discrimination memories acquired in the absence of the hippocampus, J. Neurosci. 41 (11) (2021) 2437–2446.
[71] P.W. Frankland, et al., The dorsal hippocampus is essential for context discimination but not for contextual conditioning, Behav. Neurosci. 112 (4) (1998) 863–874.
[72] K.A. Dougherty, T. Islam, D. Johnston, Intrinsic excitability of CA1 pyramidal neurones from the rat dorsal and ventral hippocampus, J. Physiol. 590 (22) (2012) 5707–5722.
[73] C. Pandis, et al., Differential expression of NMDA and AMPA receptor subunits in rat dorsal and ventral hippocampus, Neuroscience 140 (1) (2006) 163–175.